Dam-break dry granular flows: experimental and numerical analysis

STEFANIA EVANGELISTA, GIOVANNI DE MARINIS, CRISTIANA DI CRISTO, ANGELO LEOPARDI
Dipartimento di Ingegneria Civile e Meccanica
Università di Cassino e del Lazio Meridionale
via G. Di Biasio, 43, 03043 Cassino (FR)
ITALY
s.evangelista@unicas.it http://www.docente.unicas.it/stefania_evangelista

Abstract: - Granular flows have been the subject of several researches in the last years, not only in fluvial hydraulics and risk management but also in many other engineering applications, such as, for instance, material stockpiling and freights, food manufacturing and industrial processes.
This research is aimed at giving a contribution in the comprehension of such phenomena, through the analysis of the results of a specific campaign of small-scale laboratory experiments of dry granular flows produced by dam breaks conducted in the Laboratory of Water Engineering (LIA) at University of Cassino and Southern Lazio, Italy, and of their numerical simulations.
Tests have been performed with two different sands and different initial material heights in the reservoir. They provided data available for the validation of numerical models describing granular flows. Moreover, they may be used also for testing morphodynamic models adopted for the simulation of fluvial hydraulic processes in order to verify their capability of reproducing the behavior of the only solid phase. A depth-integrated two-phase model, originally developed for sediment transport in unsteady flows, is herein adopted to simulate the presented experiments. To this aim only the equations related to the solid phase are considered. The presented numerical results show a reasonable agreement with the final configurations of the dry granular dam breaks experimentally observed.

Key-Words: - Dry granular, dam break, debris flows, laboratory experiments, numerical simulations, risk management

1 Introduction

Dam-break flows have been widely investigated, from theoretical, numerical and experimental standpoints (e.g. [1], [2], [3]) especially in the clear water case ([4], [5]) but also in the presence of erodible bottoms, when sediment transport and bed evolution deeply affect the phenomena (e.g. [3], [6]). Dam breaks considering different fluids, sediment mixtures or granular materials have also been investigated (e.g. [7], [8]).

Granular flows have been the subject of several researches in the last years, justified by a deep interest in better understanding lots of natural and men-induced phenomena, being these flows related to many engineering applications. Studies of flows of granular material are of great importance, for instance, in the fields of disaster prevention and risk management with reference to natural large-scale events, such as landslides and debris flows. The safety management of a community requires to deepen the current knowledge of such topics, so to implement measures and activities aimed at preventing or reducing the big impacts of natural disasters on humans and their assets [9]. This necessity is growing especially in the last years, since the risk of potential occurrence of such events is significantly increased due to recent climate changes [10] and intensive anthropic intervention with its negative aspects (e.g. [11]). Granular flows constitute an interesting issue also in material stockpiling and freights, food manufacturing and industrial processes.

The dynamic behavior of a granular cluster depends on the peculiar characteristics of the moving material. Different rheological models have been adopted in order to reproduce the experimental evidences for different materials ([12], [13]).

It is interesting, however, to investigate the analogies in the evolution of waves arising from the fast opening of a gate trapping a fluid or granular material, along with the possibility of applying the modeling approach adopted in the clear-water case to granular flows [14]. This aim motivates the present research. Granular materials exhibit, in several physical phenomena, a fluid-like behavior, which is strongly dissipative due to friction and inelastic collisions. A first study in this field was conducted by [15], who investigated the behavior of spherical particles, in laminar, homogeneous and steady conditions, by means of a simplified conceptual model completed with experimental analyses.

Significant progresses in understanding the dynamics of granular flows have been made through the study of steady flows down a slope using depth-averaged equations and reproducing in different ways the effect of friction ([16], [17], [18]). As for transient cases, some experiments have been conducted with the instantaneous release of a cylindrical column of dry granular material on a horizontal plane ([19], [20]). Despite the complexity of the dynamics, simple scaling laws have been found to describe the final deposit configurations. Experimental investigations on two-dimensional (2D) dam breaks are reported in [21], [22], [23], considering different dry granular materials. [24] compared dam-break experiments realized with water, fluidized and dry granular flows, showing a water-like behavior of initially fluidized granular flows, with meaningful differences respect to the dry material.

Several attempts have also been made to describe granular dam breaks through mathematical models. The main problem when modeling these phenomena is related to the expression of resistances. In dry granular flows particle interactions, such as friction and collisions, are the dominant source of energy dissipation. [25] proposed a shallow-water model with a Coulomb-base friction stress and a pressure coefficient, which incorporates the effect of the internal material friction. [26] also proposed a shallow granular-flow model, in which resistance are assumed to derive from a Coulomb-like friction and a collisional stress.

In the present work, the behavior of a granular material in a fast transient situation on an horizontal surface is experimentally investigated. In particular, cohesionless dry grains, without interstitial fluid effect, are considered. The experimental campaign has been conducted in the Laboratory of Water Engineering (LIA) at University of Cassino and Southern Lazio, Italy. Small-scale laboratory experiments of dry granular dam breaks have been performed reproducing the sudden collapse by abruptly removing the retaining wall of the sand grains in a rectangular channel. Different tests have been performed starting from different initial sand heights and using two different almost-uniform sands.

The main objective is to furnish further experimental observations of 2D dam-break dry granular flows. The presented new data are elaborated in order to analyze the scaling and the geometrical dependence proposed in literature. The normalized results have been compared against the ones obtained by [22] performing similar experiments, in order to light similarities and differences.

Furthermore, dry granular flows experiments may also represent an important test for morphodynamic models adopted for the simulation of fluvial hydraulic processes (e.g. [27], [28]). The robustness of such models is often verified in clear-water conditions; conversely, in this article it is suggested that the capability of reproducing the behavior of the only sediments has to be verified too. The depth-integrated two-phase model, developed for unsteady morphodynamic flows by [29] is adopted here for simulating the experiments. Specifically, in the presented application only the equations relative to the solid phase are considered [30].

2 Experimental tests

A set of small-scale laboratory experiments of dry granular flows produced by dam-break have been carried out at LIA Lab in a horizontal rectangular channel with transparent walls.

The granular material is trapped by a vertical fast-opening sluice gate, thus forming a 0.40-m wide reservoir (Figure 1). The sudden removal of the gate produces the dam break flow (Figure 2).

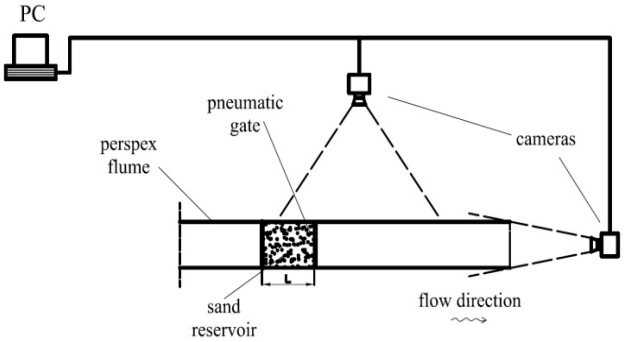

Figure 1: Sketch of the experimental equipment

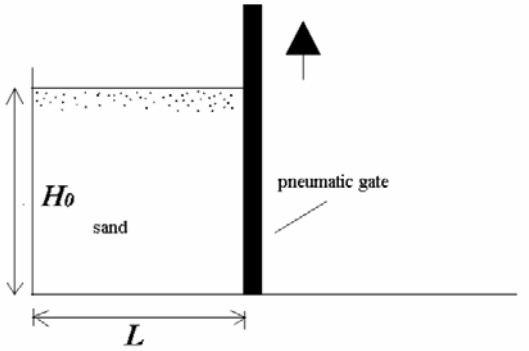

Figure 2: Sketch of the considered dam-break scheme

Two computer controlled cameras are positioned frontally and at the top of the channel, respectively, in order to record the evolution of the phenomenon during each test. The cameras have a resolution of 1360x1024 pixels and an acquisition frequency of 30 fps. For each frame the flow depth profile along the channel and the front position are evaluated through a specifically developed image analysis technique [31].

Tests have been performed with two different types of sand, both characterized by a very sharp granulometric curve; it is, therefore, acceptable to refer to the d_{50} as the characteristic diameter for each sand. Grain particles have been kept well dry in both cases, in order to reduce cohesion effect, which is here considered negligible. The "fine sand" (named "sand A") is characterized by a particle mean diameter d_{50} = 0.20 mm and a solid density ρ_s = 2680 Kg/m^3. The internal friction angle, measured through laboratory tests, is ϕ = 36°, while the estimated porosity for loose material is equal to 0.53. The "coarse sand" (named "sand B") has, instead, the following characteristics: d_{50} = 1.60 mm, ρ_s = 2560 Kg/m^3, ϕ = 41° and porosity 0.43.

As reported in Table 1, four tests for each sand are here examined, with an initial height H_0 in the reservoir varying from 0.20 m to 0.50 m. The reservoir length L is equal to 0.50 m for tests with sand A (A tests) and 0.60 m for tests with sand B (B tests), so that the reservoir height-to-base aspect ratio $r = H_0 / L$ is in the range 0.3-1.0. Each test has been repeated three times in order to verify the reproducibility of the experiments.

Table 1: Characteristics of performed tests

TEST	*Sand*	H_0 [m]	L [m]	r [-]
A1	A	0.20	0.50	0.4
A2	A	0.30	0.50	0.6
A3	A	0.40	0.50	0.8
A4	A	0.50	0.50	1.0
B1	B	0.20	0.60	0.333
B2	B	0.30	0.60	0.5
B3	B	0.40	0.60	0.667
B4	B	0.50	0.60	0.833

The front position is detected from the analysis of the images recorded from the top of the channel (Figure 3), while the longitudinal depth profile is reconstructed from the frontal camera recordings (Figure 4).

An automatic procedure making use of pre-processing and edge-detection tool software, for the fast and objective process of a great number of images, has been set up.

Numbered regular grids are attached on the frontal wall and on the channel bottom, in order to permit proper rectification and scaling of the

recorded images and, consequently, a correct measurement operation.
In this way the evolution of the time- and space-dependent processes can be properly evaluated.

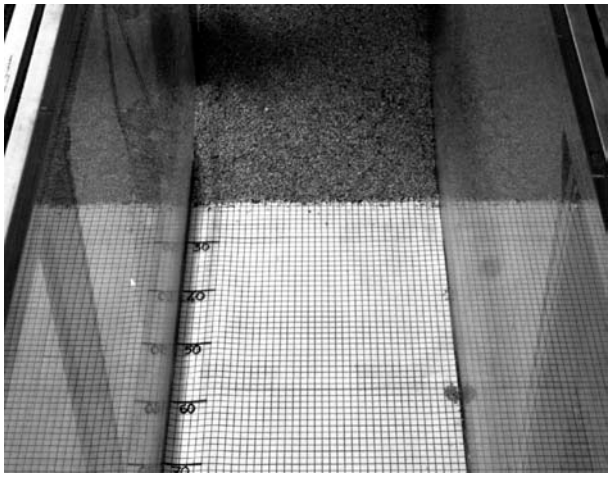

Figure 3: An image recorded from the top of the channel for the front position detection (test B1).

Figure 4: An image recorded from the front of the channel for the longitudinal profile evaluation (test A4).

For all tests, images reveal no significant wall effects on the depth, which is rather constant in the cross section, thus confirming that the flows are fairly 2D and the assumption of a 1D framework is acceptable. The longitudinal section detected from the images on the transparent front sidewall can be, therefore, assumed as representative of any other longitudinal section in the flow.

3 Experimental results

For all the performed tests, the column of sand collapses with a gradual transition from relatively-slow fracture planes, along which the grains slide down. A surface wave propagates backward in the reservoir and the backward front stops before reaching the reservoir upstream boundary, leaving a portion of mass that does not move. The wave propagating downstream stops when, at some point, a sand layer at contact with the bottom comes to a halt due to friction. As also observed by other authors (e.g. [17]), shock waves form, which bring the granular material to rest. The downward propagating wave is similar to the one that can be observed in a fluid dam break; however, in that case, the fluid keeps flowing towards the flume outlet, while for the sand the avalanche stops by friction when it reaches the bottom (or, more generally, a solid wall). When the slump comes to rest at the upward front, backward wave still propagates, in a way that the material below the shock is at or near rest, whilst the grains above the shock flow rapidly downslope, forming an avalanche of superficial layers (secondary movement).

The flow always forms a final deposit whose longitudinal extent is lower than the channel length. While the final front position is clearly defined, the final runoff is more ambiguous. In fact, it is observed that the secondary movement produces a decrease of the upper surface slope until equilibrium is reached.

The final front positions $x_{f\max}$, and its stopping time t_f, as well as the total duration of the phenomenon t_t, at which also the secondary movement is concluded, are reported in Table 2 for all the tests.

The front position is evaluated starting from the gate position, assumed as the origin of the abscissa x.

Figure 5 shows for both sands and an initial depth H_0 equal to 40 cm (tests A3 and B3) the longitudinal profiles of the sand, respectively, at the front stopping time t_f and in the final configuration, i.e. at time t_t. It can be noticed that the difference between the two profiles is more evident for sand A, for which the above-described effects of the secondary movement are more important.

A more detailed description of the experimental setup and analysis of the experimental data for sand A, also using scaling results, is reported in [26], [30] and [32], while sand B has been introduced in [33].

Table 2: Experimental data for the final front position $x_{f\max}$, front stopping time t_f and process total duration t_t for all tests

TEST	$x_{f\max}$ [m]	t_f [s]	t_t [s]
A1	0.263	0.600	1.933
A2	0.388	0.733	3.133
A3	0.518	0.900	3.666
A4	0.608	1.033	4.000
B1	0.278	0.633	1.067
B2	0.388	0.767	1.267
B3	0.518	0.867	1.567
B4	0.631	1.067	1.867

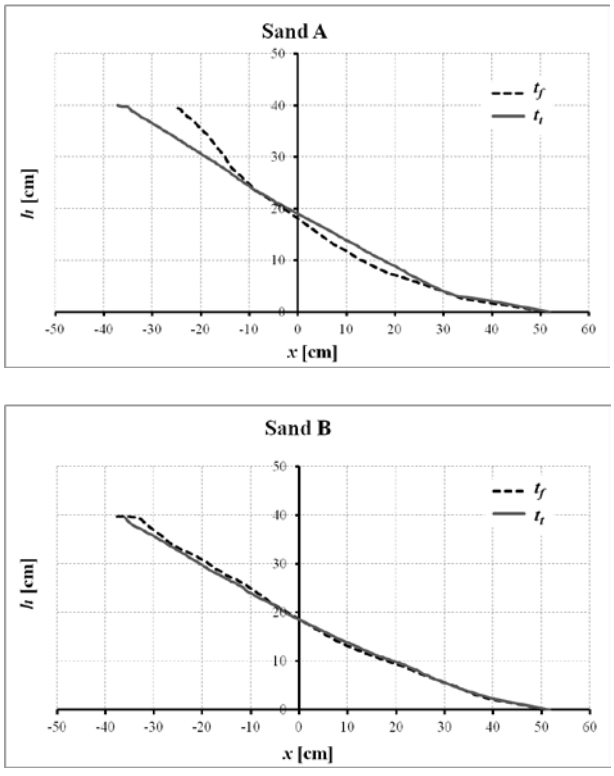

Fig. 5. Longitudinal profiles at front stopping time t_f and at the end of the phenomenon t_t for tests A3 (Sand A) and B3 (Sand B).

Figure 6 reports the same comparison between the longitudinal profiles of both sands, respectively at the front stopping time t_f and at the final time t_t, for all the presented tests. The coarse sand front is sometimes slightly advanced respect to the fine sand one. In addition, the difference between curves corresponding to different sands at equal values of H_0 is bigger at front stopping time t_f, respect to the one observed at time t_t, when the two curves are almost coincident.

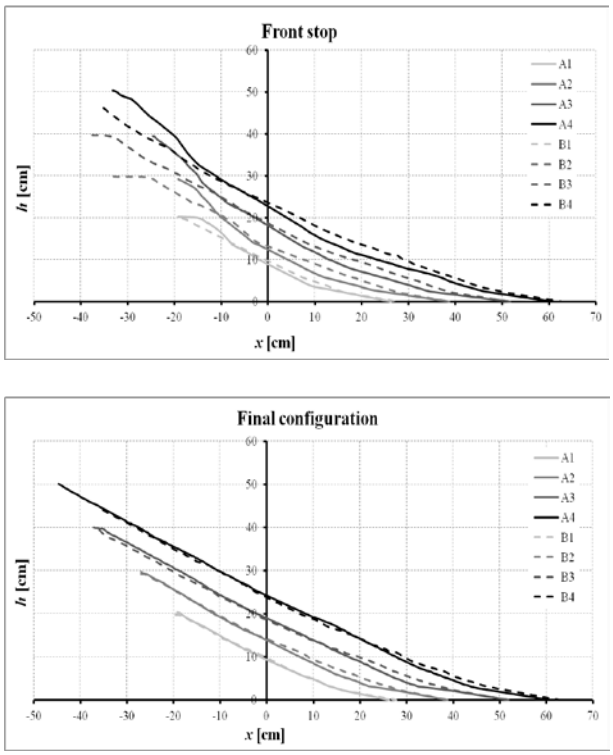

Fig. 6. Comparison between profiles at times t_f (front stop) and t_t (final configuration), respectively, for the entire set of tests.

In Figure 7, instead, the time evolution of the front position x_f is plotted for each test. It can be noticed that the front is in general more advanced for the coarse sand respect to the fine one for corresponding tests, i.e. at equal initial values of the sand height H_0 in the reservoir. The process is in general faster for sand B than for sand A, especially at the beginning of the process. At the end of the phenomenon the front position is almost the same for both sands, except for tests A1 and B1 where the difference is more evident.

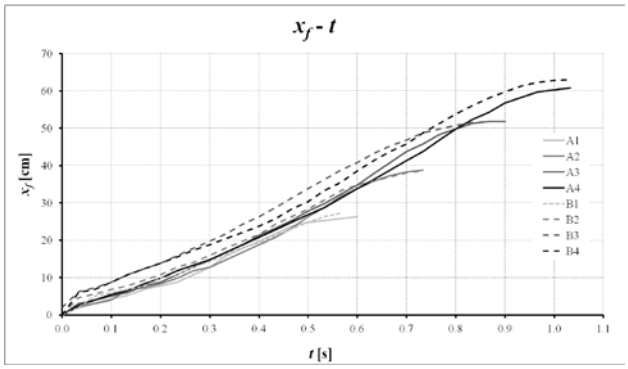

Fig. 7. Time evolution of the front position x_f for all tests.

As already observed by [24], three distinct stages can be observed: in the first phase following the collapse, the flow generated by the dam break is animated by a first constant value of the velocity, bigger than the one characterizing the second stage, which is again a constant-velocity phase; in the third phase the granular flow decelerates until stopping.

Transition between first and second phases occurs when the column height is about half its initial value; during most of the second phase, the flow height in the channel is approximately constant, except around the downstream and upstream fronts of the flow itself. Transition to the third phase occurs when the sand height has dropped to almost that of the flow in the channel, i.e. when the driving pressure between the material in the reservoir and the channel has reduced significantly.

In Figure 8 a sketch of these three stages is illustrated for the tests A1 and B1.

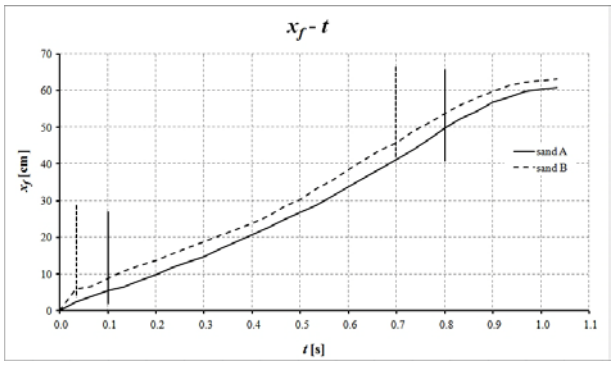

Fig. 8. Sketch of the three stages in the process evolution (tests A1 and B1).

The comparison in Figure 8, confirms that for the coarse sand the evolution of the process is in general faster respect to the fine sand one: transition from the first to the second and from the second to the third stages occur earlier for sand B than for sand A.

It is also worthy of note that, for each test, in the final configuration three different profile zones can be identified (Figure 9), differing from each other on the different values of the slope angle. Specifically, the slope values ϕ_1, ϕ_2 and ϕ_3 measured for the three zones, are, respectively, starting from upstream, in the range 28-32°, 22-26° and 11-12° for both sands. In the middle zone a smaller value of the slope can be observed for sand A (around 22.5°) respect to sand B (about 26°), while in the other ones the slope values for the two sands are more similar. Close to the bed at the front tip the smallest slope is registered, with values significantly different from the repose angle. The slope average is in general always lower than the internal friction angle of the material for both sands, as a consequence of the dynamic effects of the phenomenon. The final configuration is, therefore, not the equilibrium bank profile, defined by the repose angle, but it is strongly affected by the dynamics of the process.

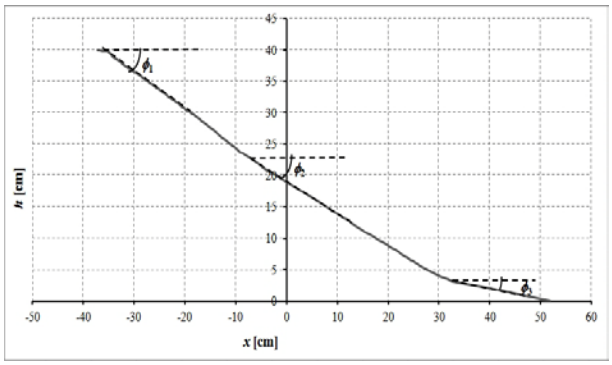

Fig. 9. Sketch of the final configuration profile.

For a better interpretation of the results, the main characterizing quantities may be considered in a dimensionless form. In particular, the following dimensionless variables are defined:

$$X = \frac{x}{H_0} \tag{1}$$

$$H = \frac{h}{H_0} \tag{2}$$

$$T = t\sqrt{\frac{g}{H_0}} \tag{3}$$

In Figure 10 dimensionless front position X_f is plotted as a function of dimensionless time T.

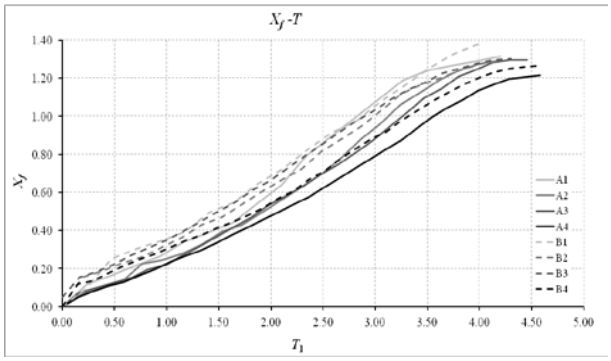

Fig. 10. Dimensionless time evolution of the front position.

The trend of front position to progress faster for sand B than for sand A, especially at the beginning of the process, is highlighted.

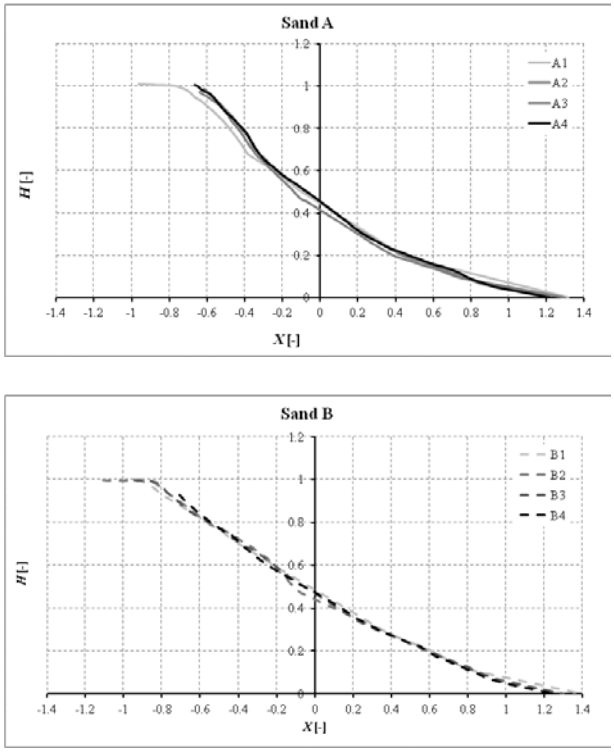

Fig. 11. Dimensionless longitudinal profile at time t_f for tests A (Sand A) and tests B (Sand B).

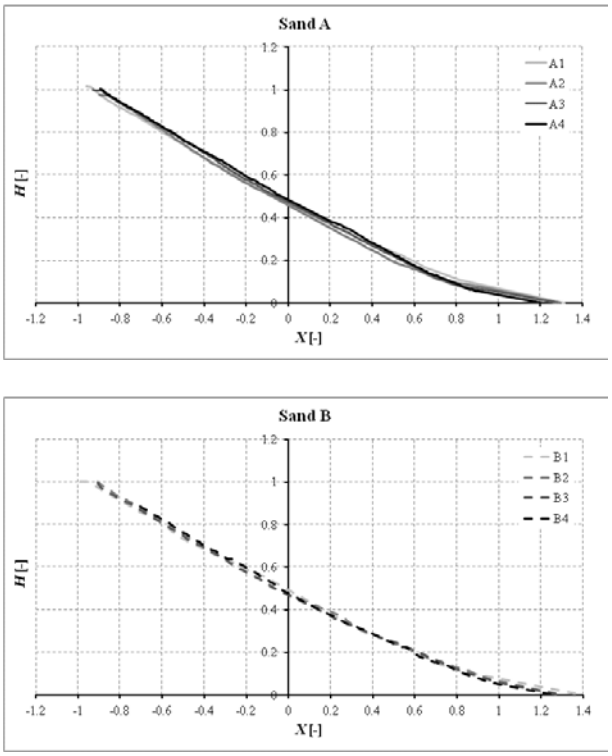

Fig. 12. Dimensionless longitudinal profile at time t_t for tests A (Sand A) and tests B (Sand B).

Dimensionless longitudinal profiles (H versus X) are plotted separately for sand A and B, respectively, first at time t_f (Figure 11) and then at time t_t (Figure 12).

In these diagrams curves appear to collapse into the same curve. The final values of dimensionless wave front position are almost the same for all tests and can be estimated equal to about X_d = 1.25. The values of the final upstream front positions are also the same and about equal to X_u = -0.84. In addition, dimensionless time at which the process ends is similar for the various tests and in the range $T = 4 \div 4.5$.

Figures 11-12 also highlight the self-similarity of longitudinal profiles at the front stopping time and at the end of the phenomenon. This self-similarity is better achieved for sand B. This is in agreement with the physical intuition that, if solid particles are big and smooth enough, the granular matter exhibits a fluid-like behavior.

Another dimensionless representation of results, which highlights better this self-similarity is the one that still scales depths h by

the initial heights H_0 (Eq.2), while horizontal lengths x are scaled by the final runout, introducing the dimensionless variable X_1 defined as:

$$X_1 = \frac{x + x_{f\max}}{x_{f\max} + x_{f\max}} \quad (4)$$

With this normalization, the front position from the gate is unity. In Figure 13, the values of the dimensionless variable H (Eq. 2), are plotted as functions of X_1 (Eq. 4), for the entire set of tests. This scaling indicates that the fractured deposits have a nearly universal shape, as already observed by [22] for similar laboratory tests. Indeed, practically the same curve is found by performing the same reduction on the data from experiments with the two different sands.

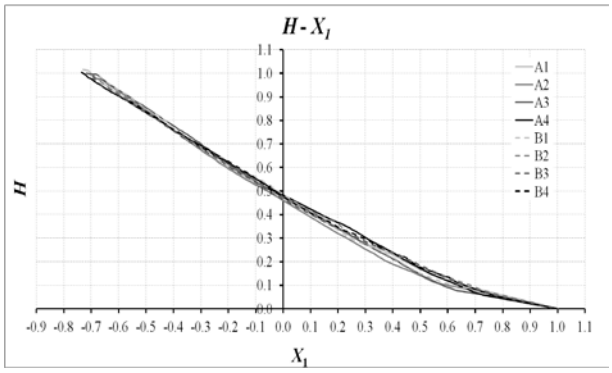

Fig. 13. Dimensionless longitudinal profiles at time t_t scaled using Eq.(2) and Eq.(4) for the highs and horizontal length, respectively.

The presented experimental results of the campaign conducted in the LIA Lab have been also compared against the ones obtained by [22]. Experiments by [22] considered a grid with mean diameter size of about 1 mm, density ρ_s = 2600 Kg/m^3, internal friction angle ϕ = 36.5° and porosity equal to 0.54 for loose material. Among the different experiments presented by the authors, the ones with aspect ratio r = 1 and r = 0.6, in the range of the values of the presented tests, have been considered. In Figure 14 the comparison with longitudinal profiles of all tests for sand A and B is plotted considering the dimensionless variables H and X. The self-similarity is confirmed, despite the grain size differences.

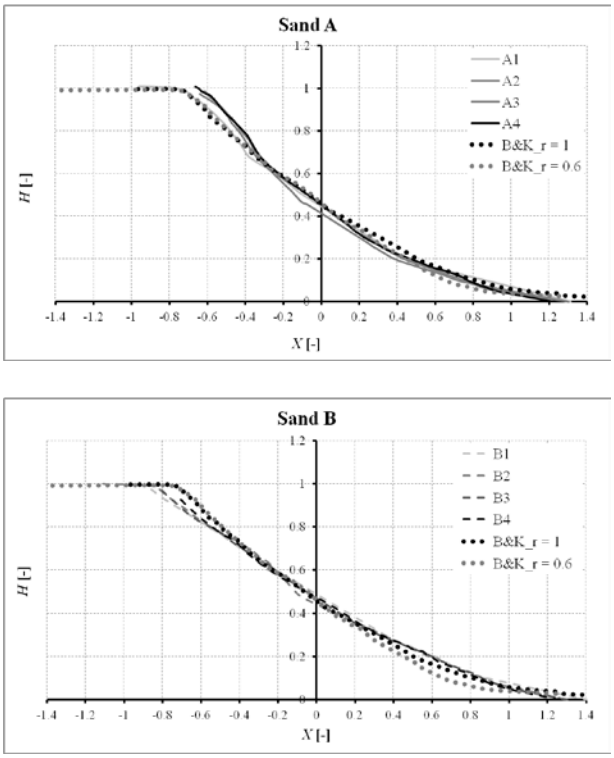

Fig. 14. Comparison of dimensionless longitudinal final configuration profiles obtained for tests A (Sand A) and tests B (Sand B) with the ones of the experiments conducted by [22].

4 The numerical model

The depth-integrated model proposed by [29] expresses mass and momentum conservation equations for both water and solid phases. Only the ones relative to the solid phase are here considered for the application to granular flows.

On the assumption of a hydrostatic pressure distribution and considering a layer of material flowing over a rigid surface, conservation of mass and momentum are expressed by:

$$\frac{\partial h}{\partial t} + \frac{\partial hu}{\partial x} = 0 \quad (5)$$

$$\frac{\partial hu}{\partial t} + \frac{\partial}{\partial x}\left(hu^2 - g\frac{h^2}{2}\right) - ghS_0 + \frac{\tau_T}{\rho_s} = 0 \quad (6)$$

where x is the streamwise coordinate, t is time, g is gravity, h the layer depth, u the flow velocity, S_0 the bottom slope, ρ_s the material density and τ_T the total stress [30].

In the case of mixture of non-cohesive coarse fraction, the dissipation mechanism is

influenced by two prevalent regimes ([34], [35]): (a) a quasi-static regime, in which long-term contacts producing rubbing and sliding between particles occur; (b) a collisional regime, where the contacts are of short duration [15]. The total stress τ_T is, therefore, written as the sum of two terms:

$$\tau_T = \tau_s + \tau_b = c_0 \rho_s \alpha u^2 + \rho_s g h \tan\phi \qquad (7)$$

the collisional shear stress τ_s, expressed as the product of the squared velocity u, the Bagnold's coefficient α and the material bulk density $c_0\,\rho_s$, being c_0 the volume fraction, and the frictional shear stress τ_b, expressed by the Coulomb friction law, being ϕ the friction angle. It is worth of note that the τ_b term does not represent just the resistance on the bottom, because it is a depth-integrated shear stress. In this framework, the friction angle constitutes an important parameter of the model.

Equations (5) and (6) represent a system of conservation laws in the variables h and u. The investigation of the mathematical nature of the model reveals the existence of two real and distinct eigenvalues:

$$\lambda_{1,2} = u\left(1 \pm \frac{1}{F_r}\right) \qquad (8)$$

with $F_r = u/(gh)$ and, therefore, that the system is always hyperbolic.

The mathematical model has been numerically integrated using the GMUSTA scheme ([36], [37], [38]), a first-order multi-stage centered scheme [6].

5 Comparison between experimental and numerical results

Some numerical results, specifically in terms of longitudinal profiles in the final configuration (at time t_t) are plotted in Figure 15 in comparison with the experimental results for sand A and B.

Simulations have been run with a time step Δt = 0.0001 s and a grid size Δx = 0.001 m. Besides the sand physical parameters (density, mean diameter, porosity and friction angle), assigned as measured in laboratory, it is necessary to fix as model parameter the Bagnold coefficient, chosen equal to 1.2 and 0.4, respectively, for sand A and B.

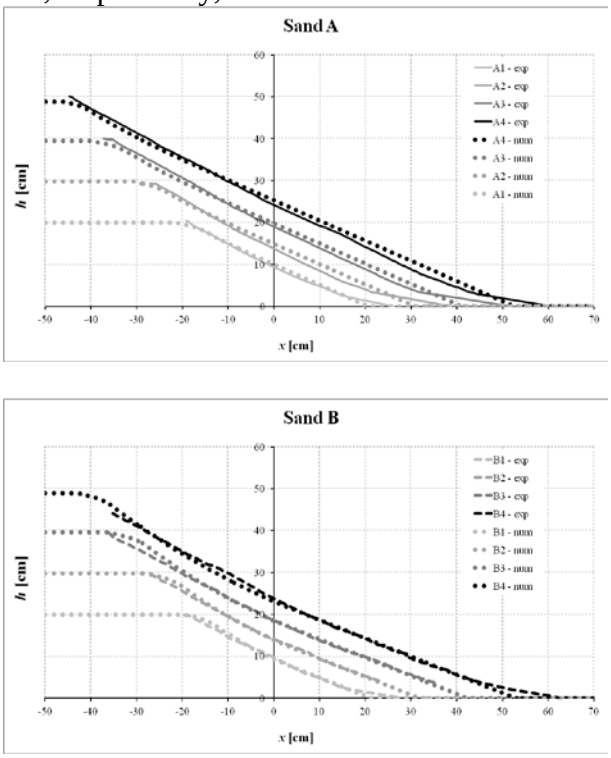

Fig. 15. Comparison between experimental and numerical results in terms of longitudinal profiles at time t_t for tests (Sand A) and tests B (Sand B).

The comparison shows a reasonable agreement between numerical and experimental results for each test.

Slight discrepancies between the two curves can be observed especially in the positions of the two fronts (upstream and downstream ones), although they are more evident for the downstream front. These differences are probably due to the dynamic effects of the process, which, as previously observed, modify the actual values of the friction angle ϕ. The model equations, instead, refer to the repose angle of the sand, considered constant for each material during the evolution of the phenomenon. It is also observed that the differences between the observed and the predicted data are more pronounced for sand A, as expected being the secondary movement, not properly taken into account in the numerical model, more important. Further developments can be implemented on the numerical model in

order to account for these features and better reproducing the process evolution.

6 Conclusions

In this work small-scale experimental results of dry granular flows produced by dam breaks have been presented. Tests have been conducted on two different kinds of non-cohesive sands, starting from different initial sand levels in the reservoir. Longitudinal sand profile and wave front positions have been evaluated for each test at different times through an ad-hoc image-analysis procedure. Results highlighted the existence of a secondary movement which affects the phenomenon evolution and is more evident for the finer sand. The longitudinal profile slope is on the average smaller than the sand internal friction angle for both materials, due to the dynamical effects characterizing the process. The coarser sand, for the same initial depth in the reservoir, shows a faster progress with time. A self-similarity of final longitudinal profiles is also observed.

The presented experimental results represent a useful dataset for the validation of numerical models of granular matter flows. In this context, a depth-averaged two-phase model, with reference to the only equations pertinent to the solid phase, has been adopted for numerical simulations of the experiments. Results show a reasonable agreement with the experimental evidence.

References:

[1] Lauber G., & Hager W.H., Experiments to dambreak wave: horizontal channel. *J. of Hydr. Res.*, IAHR, Vol.36, No.3, 1998.

[2] Chanson H., Applications of Saint-Venant equations and method of characteristics to dam break wave problem, *Report CH55/05*, Department of Civil Engineering, University of Queensland, 2005.

[3] Spinewine B., & Zech Y., Small-scale laboratory dambreak waves on movable beds, *Journal of Hydraulic Research*, Vol.45 Extra Issue, 2007, pp. 73-86.

[4] Ritter A., Die Fortpflanzung der Wassarwellen. *Z. Vereines Deutsh. Ing.*, Vol.36, No.33, 1892, pp.947-954 (in German).

[5] Stoker J.J., *Water waves*, Interscience Publishers Inc., Wiley and Sons, New York, N.Y., 1957.

[6] Evangelista S., Altinakar M., Di Cristo C. & Leopardi A., Simulation of dam-break waves on movable beds using a multi-stage centered scheme, *Int. Journal of Sediment Research*, Vol. 28, No. 3, 2013, pp.269-284, DOI: 10.1016/S1001-6279(13)60039-6.

[7] Frenette R., Zimmermann T., Eyheramendy D., Unified modeling of fluid or granular flows on dam-break case, *J. of Hydr. Eng*, ASCE, Vol.128, No.3, 2002, pp.299-305.

[8] Chanson H., Jarny S., & Coussot P., Dam break of thixotropic fluid, *J. of Hydr. Eng*, ASCE, Vol.132, No.3, 2006, pp.280-293; DOI:10.1061 /(ASCE) 0733-9429.

[9] Prochazkova D., Natural Disasters´ Management and Detection of Priority Problems for Future Research, *WSEAS Transactions on Environment and Development*, Vol. 10, 2014, pp.1-14.

[10] Parry M. L., Canziani O. F., Palutikof J. P., van der Linden P. J. & Hanson C. E., Climate Change 2007: Impacts, Adaptation and Vulnerability. Contribution of Working Group II to the Fourth Assessment *Report* of the Intergovernmental Panel on Climate Change, Cambridge University Press, Cambridge, UK, 2007, 982pp, ISBN 978 0521 88010-7.

[11] Murarescu O.-M., & Pehoiu G., Environmental impact of landslides in sub-Carpathian area between the valleys of the rivers Dâmbovița and Prahova (Romania). *WSEAS Transactions on Environment and Development*, Vol.2 No.6, 2010, pp.73-82.

[12] Hutter K., Svendsen, B., Rickenmann, D., Debris flow modeling: A review, *Continuum Mech. Thermodyn.*, Vol. 8, 1996, pp.1-35.

[13] Iverson, R. M., The physics of debris-flows, *Review of Geophysics*, Vol.35, No.3, 1997, pp.245-296.

[14] Ghilardi, P., Pagliardi, M., Biancardi., A., Flussi granulari innescati dalla rimozione rapida di una paratoia, *Proc. of Convegno Nazionale di Idraulica*, settembre 2004, Trento.

[15] Bagnold R.A, Experiments on a gravity-free dispersion of large solid spheres in a Newtonian fluid under shear, *Proc. Roy. Soc*, Vol.225, 1954, pp.49-63.

[16] Savage S.B., & Hutter K., The motion of a finite mass of granular material down a rough incline. *J. Fluid Mech.*, Vol.199, 1989, pp. 177-215.

[17] Gray J.M.N.T., & Hutter K., Pattern formation in granular avalanches, *Continuum Mech. Thermodyn.*, Vol.9, 1997, pp.341–345.

[18] Pouliquen O., Scaling laws in granular flows down rough incline planes, *Phys. Fluids*, Vol.11, No.3, 1999, pp.542-548, DOI: S1070-6631(99) 00603-0.

[19] Lube G., Huppert H.E., Sparks R.S.J., Hallworth M.A., Axisymmetric collapses of granular columns, *J. FluidMech.*, Vol.508, 2004, pp.175-199; DOI: 10.1017/S002211 2004 009036.

[20] Lajeunesse E., Mangeney-Castelnau A., & Vilotte J.P., Spreading of a granular mass on a horizontal plane, Phys. Fluids, Vol.16, No.7, 2004, pp.2371-2381.

[21] Lube G., Huppert H.E., Sparks R.S.J., Freundt, A, Collapses of two dimensional granular columns, *Phys. Rev. E,* 72, 2005, DOI: 10.1103/PhysRevE.72.041301.

[22] Balmforth N.J., & Kerswell R.R., Granular collapse in two dimension, *J. Fluid Mech.*, Vol.538, 2005, pp.399-428, DOI:10.1017/S00 22112005005537.

[23] Sarno L., Papa M. N. & Martino R., Dam-break flows of dry granular material on gentle slopes, Rinaldo Genevois, Douglas L. Hamilton, Alberto Prestininzi *5th International Conference on Debris-Flow Hazards Mitigation, Mechanics, Prediction and Assessment*, 2011, pp.503-512, Roma, Ed. Università La Sapienza. ISBN:9788895814469 ID:3093991.

[24] Roche O., Montserrat, S., Nino, Y., Tamburrino, A. Experimental observations of water like behavior of fluidized, dam break granular flows and their relevance for the propagation of ash-rich pyroclastic flows. *J. of Geophys. Res.*, Vol.113, 2008, pp.1-15; DOI:10.1029/2008JB005664.

[25] Kerswell R.R., Dam break with coulomb friction: a model for granular slumping, *Phys. Fluids*, Vol.17, 2005, DOI:10:1063/1.1870592.

[26] Di Cristo C., Vacca A., & de Marinis G., Analytical solution of dam break wave in dry granular flows, *Proc. of the 1st European IAHR Congress*, Edimburgh (UK) , 2010.

[27] Graf W.H. with Altinakar M., *Fluvial Hydraulics: Flow and Transport Processes in Channels of Simple Geometry*, John Wiley & Sons, 1998.

[28] Greco M., Iervolino M., Leopardi A. & Vacca A., A two-phase model for fast geomorphic shallow flows, *Int. Journal of Sediment Research*, Vol.27, No.4, 2012, pp.409-425, DOI:10.1016/S1001-6279(13)60001-3.

[29] Greco M., Iervolino M., Leopardi A., & Vacca A., A two-phase model for sediment transport and bed evolution in unsteady river flow, *Proc. of the Int. Conf. RiverFlow 2008*, Cesme Turkey, 2008, Vol.1, pp.669-677.

[30] Di Cristo C., Leopardi A., & Greco M. (2010). Modeling dam break granular flow. *Proc. of Int. Conf. River Flow 2010*, Braunschweig, Germany, September 8-10, 2010, Vol.1, pp.577-583, ISBN/ISSN: 9783939230007.

[31] Grimaldi L., Dam Break di materiale granulare secco, *M.Sc. Thesis in Civil Engineering*, Università di Cassino e del Lazio Meridionale, Supervisor Stefania Evangelista.

[32] Evangelista S., Di Cristo C., & de Marinis G., Experiments and simulations of dam break over fixed and granular beds, *Proc. of the Int. XXXV IAHR Biennal Congress*, Brisbane, Australia, 26 June-1 July, 2011, pp.3450-3457, ISBN: 9780858258686.

[33] Evangelista S., de Marinis G., Di Cristo C., Leopardi A. & Grimaldi L., Experimental study of dam-break dry granular flows, Proc. of the *7th WSEAS International Conference on Engineering Mechanics, Structures, Engineering, Geology* (EMESEG '14), Special session "Analysis and modelling of fast-moving flow-like phenomena", Salerno, Italy, June 3-5, 2014, ISBN/ISSN: 978-960-474-376-6.

[34] Johnson P.C. & Jackson R., Frictional-collisional costitutive relations for granular materials, with application to plane shearing. *J. Fluid Mech*, Vol.176, 1987, pp.67-93.

[35] Johnson P.C., Nott P. & Jackson R., Frictional-collisional equations of motion for particulate flows and their application to chutes, *J. Fluid Mech.*, Vol. 210, 1990, pp.501-535.

[36] Toro E. F., MUSTA: A multi-stage numerical flux, *Applied Numerical Mathematics*, Elsevier Science, 2006, Vol.56, pp.1464-1479.

[37] Toro E. F. & Titarev V. A., Derivative Riemann solvers for systems of conservation laws and ADER methods, *Journal of Computational Physics*, Elsevier Science, 2006a, Vol.212, pp.150-165.

[38] Toro, E. F. & V. A. Titarev, MUSTA fluxes for systems of conservation laws, *Journal of Computational Physics*, Elsevier Science, 2006b, Vol.216, pp.403-429.